Infrared spectra of annite in the OH-stretching vibrational range

Autor(en): **Boukili, Boubker / Holtz, François / Robert, Jean-Louis**

Objekttyp: **Article**

Zeitschrift: **Schweizerische mineralogische und petrographische Mitteilungen = Bulletin suisse de minéralogie et pétrographie**

Band (Jahr): **83 (2003)**

Heft 3

PDF erstellt am: **06.08.2024**

Persistenter Link: https://doi.org/10.5169/seals-63153

Schweizerische Mineralogische und Petrographische Mitteilungen 83, 331–340, 2003

Infrared spectra of annite in the OH-stretching vibrational range

Boubker Boukili[1], François Holtz[2], Jean-Louis Robert[3], Mohammed Joriou[4], Jean-Michel Bény[3] and Mohamed Najt[1]

Abstract

In the OH-stretching range, most of the micas studied exhibit partial dioctahedral character, which increases with increasing fO_2. At both the Ni-NiO and wüstite-magnetite oxygen buffers, our spectra of annite indicate the presence of aluminum and Fe^{3+} in octahedral sites, which is required to articulate the octahedral layers. The decomposition of the infrared spectra allows one to redefine the assignment of annite absorption bands. Three V-bands of "dioctahedral-type" (in the range 3580–3520 cm^{-1}) are characterized by the bulk number of charges of the two adjacent cations: two bands due to OH groups adjacent to an octahedral vacancy and bonded to $Fe^{2+}Al^{3+}\square$ or $Fe^{2+}Fe^{3+}\square$ (range 3580–3540 cm^{-1}); a band due to OH groups bonded to $Fe^{3+}Fe^{3+}\square$ at 3530 cm^{-1}. For Al-rich annite, the band assigned to OH–$Fe^{2+}Fe^{3+}\square$ is replaced by a band due to OH groups adjacent to $Fe^{3+}Al^{3+}\square$. An 8-fold charged environment OH–$Fe^{2+}Al^{3+}Al^{3+}$ does not seem likely in the micas studied. At higher wavenumbers, two I-bands of "trioctahedral-type" (OH–$Fe^{2+}Fe^{2+}Fe^{3+}$ and $Fe^{2+}Fe^{2+}Al^{3+}$) and one N-band corresponding to OH–$Fe^{2+}Fe^{2+}Fe^{2+}$ have been resolved. For all trioctahedral-type bands (I- and N-bands), a systematic shift is observed toward lower wavenumbers with increasing aluminum content of the mica. When compared to N- or I-bands, V-bands show an opposite behaviour.

Keywords: Annite, ferrous aluminous biotites, OH-stretching vibrations, 8-fold charged, OH-groups.

Introduction

Vibrational spectroscopic techniques, in particular infrared spectroscopy, are efficient tools to understand the relation between structure and local chemistry of phyllosilicates, particularly biotites. Annite $\{K\}[Fe]_3<Si_3Al>O_{10}(OH)_2$ is the theoretical iron end-member of the trioctahedral biotite solid solution and one of the major components of natural biotites. The spectroscopic characterization of this end-member composition is of particular importance. A general correlation between the frequency of modes attributed to the OH-stretching vibrations and compositional variations of micas has been proposed by Robert and Kodama (1988) for micas in the system K_2O–MgO–Al_2O_3–H_2O. However, in the Fe-bearing system there is controversy in the assignment of OH-stretching bands. Indeed, Redhammer et al. (2000) adopted the model proposed by Robert and Kodama (1988) to assign OH-bands in Fe-Al-rich biotites, leading to the possible existence of 8-fold charged environments for OH-groups, which is surprising and not common in micas. In addition, this model which has been established for magnesium micas could not distinguish between the OH-groups adjacent to vacant sites (V-bands of dioctahedral-type). Thus, the assignment made by Redhammer et al. (2000) needs to be reconsidered, particularly for V-bands. In this study, syntheses of annite and ferrous-aluminous biotites have been performed at two oxygen fugacities to constrain and re-examine the assignments of OH-bands in annite infrared spectra.

Starting compositions

To synthesize micas along the annite-siderphyllite join, various gels were prepared according to the method of Hamilton and Henderson (1968). These gels were used as starting material for hydrothermal synthesis of micas. Potassium was introduced as dry K_2CO_3, silicon as tetraethylorthosilicate (TEOS), aluminum and one part of iron (50%) as nitrate. Finally, metallic iron Fe° (50%)

[1] Faculté des sciences de Rabat, Département des sciences de la Terre, UFR geoappl, BP 1014, Rabat, Maroc. <boukili@fsr.ac.ma>
[2] Universität Hannover, Institut für Mineralogie, Welfengarten 1, D-30167 Hannover, Germany.
[3] CNRS-CRSCM, Orléans, 45071-cedex 02, France.
[4] Faculté des sciences Fès, UFR signaux BP 2202, Fès, Maroc.

0036-7699/03/0083/331

was mechanically added to the gels to obtain the appropriate bulk compositions.

The compositions of trioctahedral micas studied are expressed by:

$$\{K\}[Fe_{3-x}Al_x]<Si_{3-x}Al_{1+x}>O_{10}(OH)_2$$

where x corresponds to the extent of the Tschermak-type substitution. In the following text, annite and siderophyllite refer to the compositions with x equal to 0 and 1.

Experimental methods and analytical procedures

The syntheses were done in Tuttle-type externally heated pressure vessels working vertically, with water as the pressure medium. Temperature was measured using Ni-NiCr thermocouples calibrated against the melting points of NaCl and $ZnCl_2$ yielding temperature uncertainty of less than ±5 °C. Pressures were measured with a bourdon

Table 1a Experimental products obtained at 600°C, NNO buffer and 1 kbar along the join annite-siderophyllite. Interplanar distances are measured at ±0.0004 Å. dt is the average cation-anion distance calculated from the relation proposed by Hazen and Burnham (1973): dt = 0.163[4](Al/Al + Si) + 1.608 Å. Tetragonal rotation angles (α) are calculated from the relations of Donnay et al. (1964). The lattice parameter *b* is calculated from ($b = 6d_{060}$). The phases encountered are annite and aluminous biotite (Al-biotite), mica (mc), magnetite (mt), spinel (sp), corundum (cor) and kalsilite (ks). [4](Al/Al + Si) is the bulk atomic aluminum fraction of the starting gels.

Starting compositions	Phases obtained	d_{060} (Å)	*b* (Å)	[4][Al/(Al+Si)]	dt (Å)	α (°)
annite (x = 0)						
$\{K\}Fe_3<Si_3Al>O_{10}(OH)_2$	mc + san + mt	1.5534	9.3204	0.25	1.6487	2.11
$\{K\}Fe_{2.9}Al_{0.1}]<Si_{2.9}Al_{1.1}>O_{10}(OH)_2$	mc + san + sp	1.5521	9.3126	0.275	1.6528	5.11
$\{K\}[Fe_{2.8}Al_{0.2}]<Si_{2.8}Al_{1.2}>O_{10}(OH)_2$	mc + san + sp	1.5517	9.3102	0.30	1.6569	6.62
$\{K\}[Fe_{2.7}Al_{0.3}]<Si_{2.7}Al_{1.3}>O_{10}(OH)_2$	Al-biotite	1.5495	9.2970	0.325	1.6609	8.32
$\{K\}[Fe_{2.6}Al_{0.4}]<Si_{2.6}Al_{1.4}>O_{10}(OH)_2$	Al-biotite	1.5478	9.2868	0.35	1.6650	9.60
Al-biotite (x = 0.5)						
$\{K\}Fe_{2.5}Al_{0.5}]<Si_{2.5}Al_{1.5}>O_{10}(OH)_2$	Al-biotite	1.5465	9.2808	0.375	1.6691	10.60
$\{K\}[Fe_{2.4}Al_{0.6}]<Si_{2.4}Al_{1.6}>O_{10}(OH)_2$	Al-biotite	1.5449	9.2694	0.40	1.6732	11.66
$\{K\}[Fe_{2.3}Al_{0.7}]<Si_{2.3}Al_{1.7}>O_{10}(OH)_2$	Al-biotite	1.5448	9.2588	0.425	1.6772	12.61
Al-biotite (x = 0.75)						
$\{K\}Fe_{2.25}Al_{0.75}]<Si_{2.25}Al_{1.75}>O_{10}(OH)_2$	Al-biotite	1.5425	9.2550	0.4375	1.6793	13.03
$\{K\}[Fe_{2.2}Al_{0.8})]<Si_{2.2}Al_{1.8}>O_{10}(OH)_2$	mc + sp + cor + ks	1.5458	9.2748	0.45	1.6813	12.79
$\{K\}[Fe_{2.1}Al_{0.9}]<Si_{2.1}Al_{1.9}>O_{10}(OH)_2$	mc + sp + cor + ks	1.5453	9.2718	0.475	1.6854	13.47
siderophyllite (x = 1)						
$\{K\}[Fe_2Al_1]<Si_2Al_2>O_{10}(OH)_2$	mc + sp + cor + ks	1.5448	9.2688	0.50	1.6895	14.11

Table 1b Experimental products obtained at 600°C, MW buffer and 1 kbar. Parentheses (..) indicate trace amounts 1% or less of the phase present. Same remarks as for Table 1a.

starting compositions	Phases obtained	d_{060} (Å)	*b* (Å)	[4][Al/(Al+Si)]	dt (Å)	α (°)
annite (x = 0)						
$\{K\}Fe_3<Si_3Al>O_{10}(OH)_2$	annite + (san)	1.5553	9.3318	0.25	1.6487	0
$\{K\}Fe_{2.9}Al_{0.1}]<Si_{2.9}Al_{1.1}>O_{10}(OH)_2$	Al-biotite	1.5550	9.33	0.275	1.6528	3.72
$\{K\}[Fe_{2.8}Al_{0.2}]<Si_{2.8}Al_{1.2}>O_{10}(OH)_2$	Al-biotite	1.5546	9.3276	0.30	1.6569	5.63
$\{K\}[Fe_{2.7}Al_{0.3}]<Si_{2.7}Al_{1.3}>O_{10}(OH)_2$	Al-biotite	1.5436	9.3216	0.325	1.6609	7.20
$\{K\}[Fe_{2.6}Al_{0.4}]<Si_{2.6}Al_{1.4}>O_{10}(OH)_2$	Al-biotite	1.5416	9.3096	0.35	1.6650	8.73
Al-biotite (x = 0.5)						
$\{K\}Fe_{2.5}Al_{0.5}]<Si_{2.5}Al_{1.5}>O_{10}(OH)_2$	Al-biotite	1.5489	9.2934	0.375	1.6691	10.17
$\{K\}[Fe_{2.4}Al_{0.6}]<Si_{2.4}Al_{1.6}>O_{10}(OH)_2$	Al-biotite	1.5481	9.2886	0.40	1.6732	11.08
$\{K\}[Fe_{2.3}Al_{0.7}]<Si_{2.3}Al_{1.7}>O_{10}(OH)_2$	Al-biotite	1.5475	9.2850	0.425	1.6772	11.77
Al-biotite (x = 0.75)						
$\{K\}Fe_{2.25}Al_{0.75}]<Si_{2.25}Al_{1.75}>O_{10}(OH)_2$	Al-biotite	1.5454	9.2724	0.4375	1.6793	12.47
$\{K\}[Fe_{2.2}Al_{0.8})]<Si_{2.2}Al_{1.8}>O_{10}(OH)_2$	mc + sp + cor + ks	1.5459	9.2754	0.45	1.6813	12.77
$\{K\}[Fe_{2.1}Al_{0.9}]<Si_{2.1}Al_{1.9}>O_{10}(OH)_2$	mc + sp + cor + ks	1.5457	9.2742	0.475	1.6854	13.41
siderophyllite (x = 1)						
$\{K\}[Fe_2Al_1]<Si_2Al_2>O_{10}(OH)_2$	mc + sp + cor + ks	1.5440	9.2640	0.50	1.6895	14.23

Table 2 Chemical compositions as weight percent oxides of selected micas along the join annite-siderophyllite obtained from microprobe analysis.

Run	SiO_2	Al_2O_3	FeO	K_2O	Total
annite (x= 0) 600°C/NNO/1 kbar P(H_2O)	34.44	9.21	42.09	8.64	94.40
annite (x= 0) 600°C/NNO/1 kbar P(H_2O)	34.63	8.99	42.41	8.68	94.71
annite (x= 0) 600°C/MW/1 kbar P(H_2O)	35.20	9.43	42.20	8.63	95.46
Al-biotite (x= 0.5) 600°C/NNO/1 kbar P(H_2O)	30.30	20.35	34.20	9.36	94.22
Al-biotite (x= 0.5) 600°C/NNO/1 kbar P(H_2O)	30.72	20.52	35.05	9.47	95.77
Al-biotite (x= 0.5) 600°C/MW/1 kbar P(H_2O)	30.64	19.88	36.44	9.43	96.40
Al-biotite (x= 0.75) 600°C/NNO/1 kbar P(H_2O)	27.23	26.20	34.05	8.59	96.07
Al-biotite (x= 0.75) 600°C/MW/1 kbar P(H_2O)	27.36	25.95	34.04	8.70	96.05

gauge, with an uncertainty of less than ±50 bars. Experiments were performed at 600°C, 1 kbar PH_2O, with duration of 7 days. Oxygen fugacity was controlled by the double capsule method of Eugster (1957), using the magnetite-wüstite (MW) and nickel-nickel oxide (NNO) assemblages as solid buffers introduced with water in an external Au-capsule. In the inner capsule ($Ag_{70}Pd_{30}$), the gels were introduced with 15 wt% distilled water. Cooling was performed by removing the vessel from the furnace and a temperature of less than 100 °C was reached after less than 1 hour.

Some analyses of micas were done by microprobe (Cameca, SX50) in order to check the stoichiometry of the synthesized minerals. Analytical conditions were: acceleration voltage of 15 KV, initial beam current 30 nA, beam diameter 1 μm and counting time of 10 s.

The run products were examined with a petrographic microscope and by scanning electron microscopy (SEM). X-ray diffraction was used to confirm the single phase character and to characterize the micas. Diffraction patterns were obtained between $5° \leqslant 2\theta \leqslant 65°$, the radiation used was Co-Kα (λ = 1.7902 Å). The interplanar distances d_{060} (= $b/6$) were systematically measured using Si as an internal standard.

Infrared spectra (3800–3200 cm^{-1}) were recorded at room temperature on a Nicolet 710 spectrometer. Samples were prepared as KBr pellets, with a mineral to KBr ratio of 5% by weight. The resolution in peak positions is 2 cm^{-1}. The spectra were fitted to the sum of lines with Lorentzian shape using the program Peakfit. Small deviations between raw and fitted spectra were generally observed at the high-frequencies side of N-bands; this is due to the Christiansen effect (1884).

For the decomposition of the infrared spectra in the OH-stretching vibration range (3800–3200 cm^{-1}), we have adopted the nomenclature of Vedder (1964) and Robert et al. (1989) coupled to that of Boukili (1995): N-bands (also defined as Tri-6^+), due to OH groups bonded to three octahedrally coordinated divalent cations ($3Fe^{2+}$), in which the OH dipole is oriented parallel to the c* axis; I-bands (Tri-7^+), due to OH groups bonded to two divalent (Fe^{2+}) and one trivalent cation (Fe^{3+} or Al^{3+}, respectively Ia and Ib), in which the OH dipole is slightly tilted away from the c* axis; V-bands (Di-5^+or 6^+), due to OH groups adjacent to one octahedral vacancy and two octahedrally coordinated cations, in which the OH dipole is approximately within the (001) plane. The labels "Tri" and "Di" refer to trioctahedral and dioctahedral environments around the OH dipoles, while 6^+ or 7^+ indicate the bulk number of charges of the octahedral cations. Generally, the frequencies of N-type bands are the highest, and those of the V-type bands are the lowest (Robert and Kodama, 1988). The intensity of the bands resulting from dioctahedral environments around OH is much higher than that resulting from trioctahedral environments (Rouxet, 1970; Sanz et al., 1983, 1984). The intensity is higher for I-type bands than for the N-band (Rousseaux et al., 1972).

Experimental products

The products of experiments buffered by NNO assemblage (600°C, 1 kbar) with the compositions along the annite-siderophyllite join are listed in Table 1a. The products consist of mica for compositions with a value of x ranging between 0.3 and 0.75. For compositions with an x-value of 0.8 to 1, mica is found to coexist with minor amounts of spinel, corundum (identified by X-rays with the characteristic peaks of (012), (104) and (113) planes) and kalsilite (this is the maximum amount of possible phases from the phase rule).

The crystal size of mica is less than 2 μm in diameter. The micas display a brown color for the

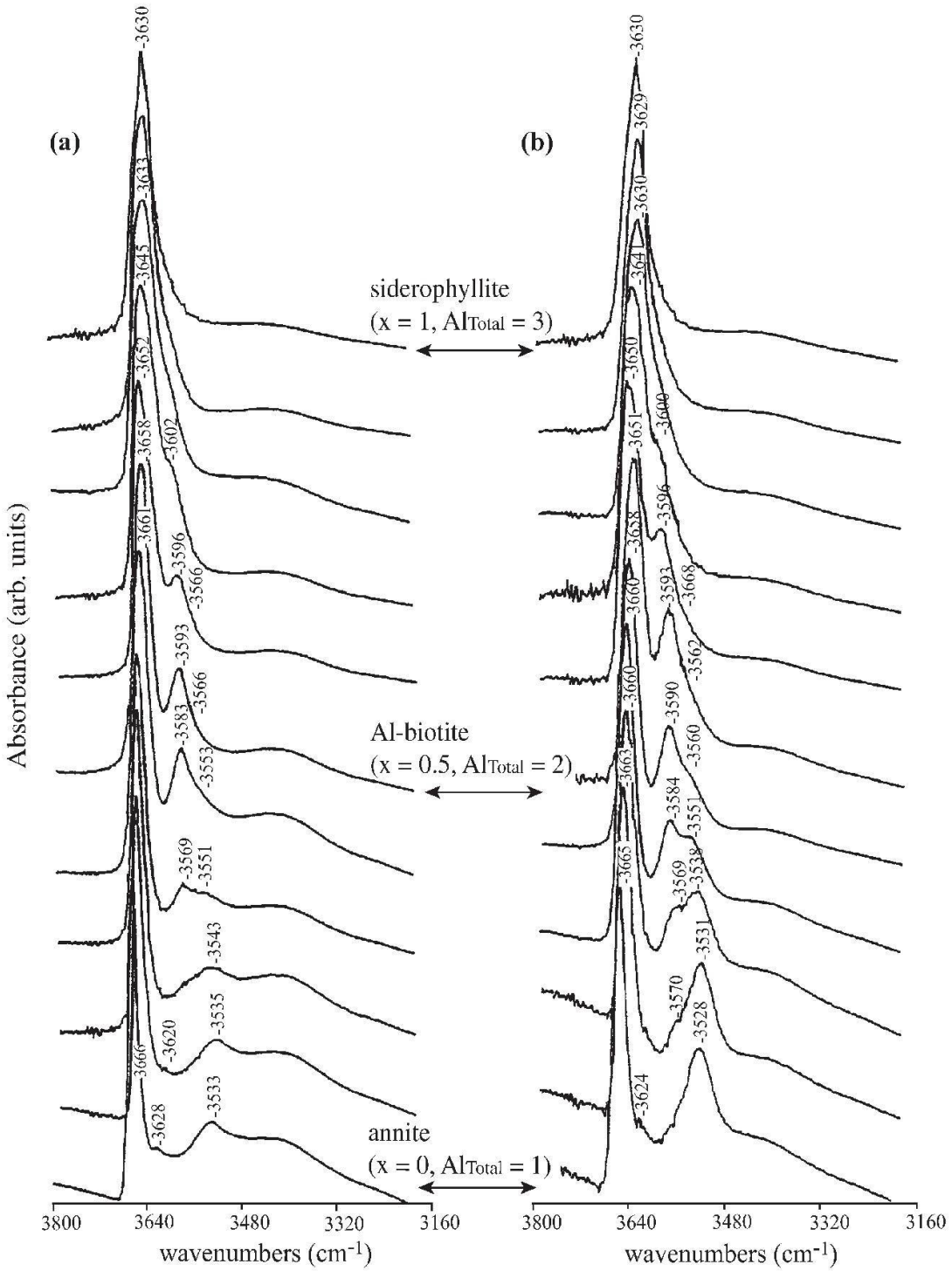

Fig. 1 Infrared absorption spectra of mica solid solutions on the join annite-siderophyllite. (a) 600°C/MW/; (b) 600 °C/NNO/ 1 kbar in the region of OH-stretching frequency range. The compositions are characterized by Al_{Total} and x which corresponds to the rate of Tschermak-type substitution.

composition with an x-value between 0 and 0.2. With increasing Al content, the mica becomes light green. The chemical analyses demonstrate that the Al-annite compositions are close to the stoichiometry of their ideal counterparts (Table 2). The offsets observed are within the expected accuracy of microprobe analyses for fine-grained particles. There is also a decrease of the interplanar distance d(060) from 1.553 to 1.542 Å with increasing x-value from 0.3 to 0.75. It can be noted that our results for Fe-rich compositions as well as those of Redhammer et al. (1993) performed at 3 and 5 kbar differ from previous studies (Eugster and Wones, 1962; Wones and Eugster, 1965; Rutherford, 1973; Nachit, 1986). In these studies, also performed at 600°C and 1 kbar, the run products were described to be mica only. This difference is probably related to the low amount of additional phases which could not be detected with the their analytical techniques. This suggests that the stabil-

ity field of Fe-rich biotites determined in these previous works needs to be reconsidered, which is in agreement with other observations (Dachs, 1994; Rebbert et al., 1995; Cyang et al., 1996). For Al-rich biotites, Redhammer et al. (2000) have shown that the solubility of Al^{3+} is strongly temperature dependent and is limited to about 0.78–0.92. Our experimental products are in good agreement with the results of Rutherford (1973) indicating that the biotite solid solution is limited to a mica with x = 0.75. For x > 0.75, this mechanism: $[^4]Si^{4+} + [^6]Fe^{2+} \Leftrightarrow [^4]Al^{3+} + [^6]Al^{3+}$ is not the only reaction of substitution. Rutherford (1973) suggests that this results from the presence of Fe^{3+} in octahedral coordination. Another explanation is a substitution of Fe by Al following the reaction: $3[^6]Fe^{2+} \Leftrightarrow 2[^6]Al^{3+} + [^6]\square$

However, following Rutherford (1973), this substitution alone cannot explain the stability limits of biotite solid solution because the maximum solid solution between annite and muscovite is limited to 10% (Monier and Robert, 1986).

The products of experiments buffered by the MW assemblage (600°C, 1 kbar) obtained from gels along the annite-siderophyllite join are listed in Table 1b and are in agreement with previous studies of ferrous-aluminous biotites (Eugster and Wones, 1962; Wones, 1963; Wones and Eugster, 1965; Rutherford, 1973; Nachit, 1986). The run products consist of mica only for compositions with a value of $x \leqslant 0.75$. For x-values of 0.8 and above, spinel, corundum and kalsilite are observed as additional solid phases. The interplanar distances decrease with increasing x-value and are lower than those buffered by NNO. These micas contain a low amount of Fe^{3+} as has been shown by Mössbauer spectroscopy (Levillain, 1982; Boukili et al., 1994; Boukili, 1995).

Infrared measurements in the OH-stretching vibrational region

The annite and Al-annite spectra are characterized by a marked peak between 3670 and 3640 cm^{-1} and by several peaks in the frequency range 3600–3500 cm^{-1} (Fig. 1). The intensity of these low frequency peaks decreases with increasing amount of Al_{Total} (or with increasing x-value).

Bands in the frequency range 3670–3620 cm^{-1}

The decomposition of spectra obtained at NNO buffer conditions is shown in Fig. 2. The high intensity peak in the frequency range 3670–3640 cm^{-1} clearly results from the contribution of two bands. In the annite spectrum the band with the highest frequency is observed at 3666 cm^{-1}. This band overlaps with a second band at approximately 3650 cm^{-1}. The band at 3666 cm^{-1} is assigned to a stretching mode of OH groups in the vicinity of the three octahedrally coordinated Fe^{2+} (Wilkins, 1967; Farmer, 1974) and is therefore an N-type band (Tri-6^+: trioctahedral environment with the bulk charge of cations = 6^+). With increasing Al_{Total} this band becomes broader (FWHM increases from 7 to 13 cm^{-1} from annite to siderophyllite) and $\nu_{OH\text{-}N}$ decreases by 20 cm^{-1} (Fig. 4). Such an evolution is the result of increasing heterogeneity of the tetrahedral layer with increasing substitution of Al in this layer (Robert, 1981; Robert and Kodama, 1988). It can be noted that the intensity of the 3666 cm^{-1} band is lower in annites synthesized at high fO_2 (NNO) compared to annites synthesized at low fO_2 (MW, see Fig. 3). The frequency of the N-type band increases from 3666 to 3669 cm^{-1} with decreasing fO_2 from NNO to MW. This may result from the presence of Fe^{3+} in the tetrahedral layer, which can be incorporated in the structural positions of Al^{3+} at oxidizing conditions.

The decompositions of spectra (Fig. 2) clearly show that the intensity of N-band (at 3666 cm^{-1} in annite) decreases and that of the 3650 cm^{-1} band increases with increasing x-value (increasing Al_{Total}). For Al-rich compositions, the intensity of this band is significantly higher than that of the N-type band. The band at 3650 cm^{-1} is therefore assigned to $OH\text{–}Fe^{2+}Fe^{2+}Al^{3+}$, an Ib-type band (Tri-$7^+$). According to Vedder (1964), the frequency decrease resulting from a change of valency from $[^6]M^{2+}$ to $[^6]M^{3+}$ is 34 cm^{-1}. This is not verified along the join annite-siderophyllite, for which a variation of $\nu_{OH\text{-}N} - \nu_{OH\text{-}Ib} = 15$ cm^{-1} is observed. However, along the join annite-siderophyllite, the change of valency is accompanied by a substitution of $[^6]Fe^{2+}$ by $[^6]Al^{3+}$. This substitution of the cation and the variation of the electronegativity of the ionic complexes associated with the hydroxyl groups (Allred and Rochow, 1958; Sanderson, 1983) explain the frequency lowering change of approximately 15 cm^{-1} between $\nu_{OH\text{-}N}$ and $\nu_{OH\text{-}Ib}$ which has been observed in several studies (e.g., Velde, 1979, 1983; Robert, 1981).

A second I-type band is observed at 3624 cm^{-1} (band Ia) for annite ($Al_{Total} = 1$) and is of low intensity. The frequency of this band decreases with increasing Al content of the mica and the band is no more detectable for micas with x-values above 0.2 ($Al_{Total} > 1.2$). Similarly to the Ib-band, the relative intensity of this band compared to that of the N-type band increases with increasing fO_2 (i.e., with increasing Fe^{3+}/Fe^{2+} ratio in the mica). Thus, this band which is sensitive to both the Fe

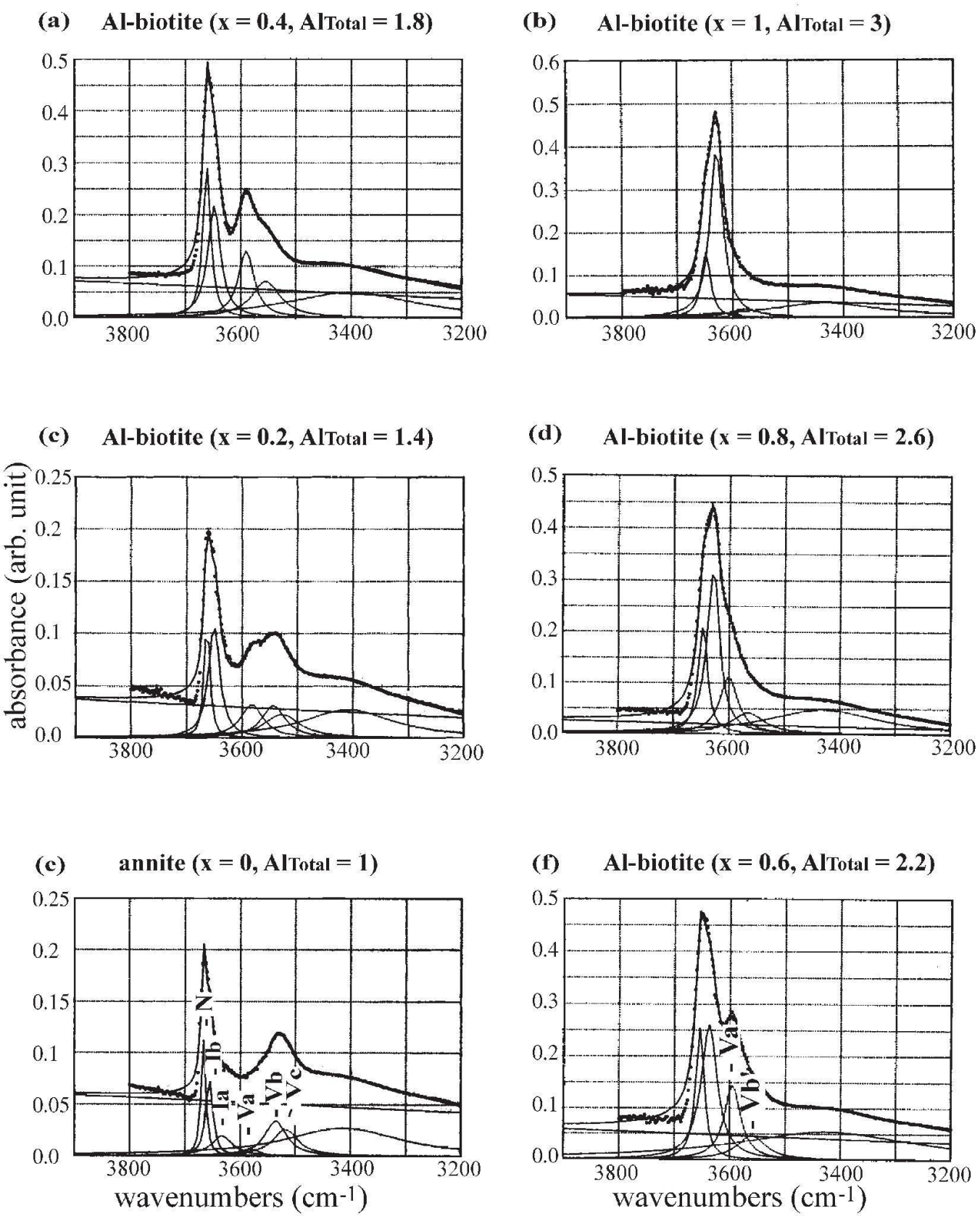

Fig. 2 Decomposed infrared spectra of micas along annite-siderophyllite join (600°C/NNO/1 kbar). N-band concerns OH bonded to $3Fe^{2+}$; Ib-band OH bonded to $Fe^{2+}Fe^{2+}Al^{3+}$; Ia—represents OH bonded to $Fe^{2+}Fe^{2+}Fe^{3+}$; Va—OH adjacent to octahedral vacancy $Fe^{2+}Al^{3+}\square$; Vb—OH bonded to $Fe^{2+}Fe^{3+}\square$; Vb'—OH-bonded to $Fe^{3+}Al^{3+}\square$; Vc—OH bonded to $Fe^{3+}Fe^{3+}\square$.

content and the Fe^{3+}/Fe^{2+} ratio of the mica must be assigned to an Ia-type band resulting from $OH–Fe^{2+}Fe^{2+}Fe^{3+}$ (Tri-$^{7+}$), as proposed by Boukili (1995) and Redhammer et al. (2000). It is emphasized that the two Ib and Ia bands in annite have not been distinguished by Redhammer et al. (1993) and Rancourt et al. (1994) and that Redhammer et al. (1993) have assigned the Ia band to

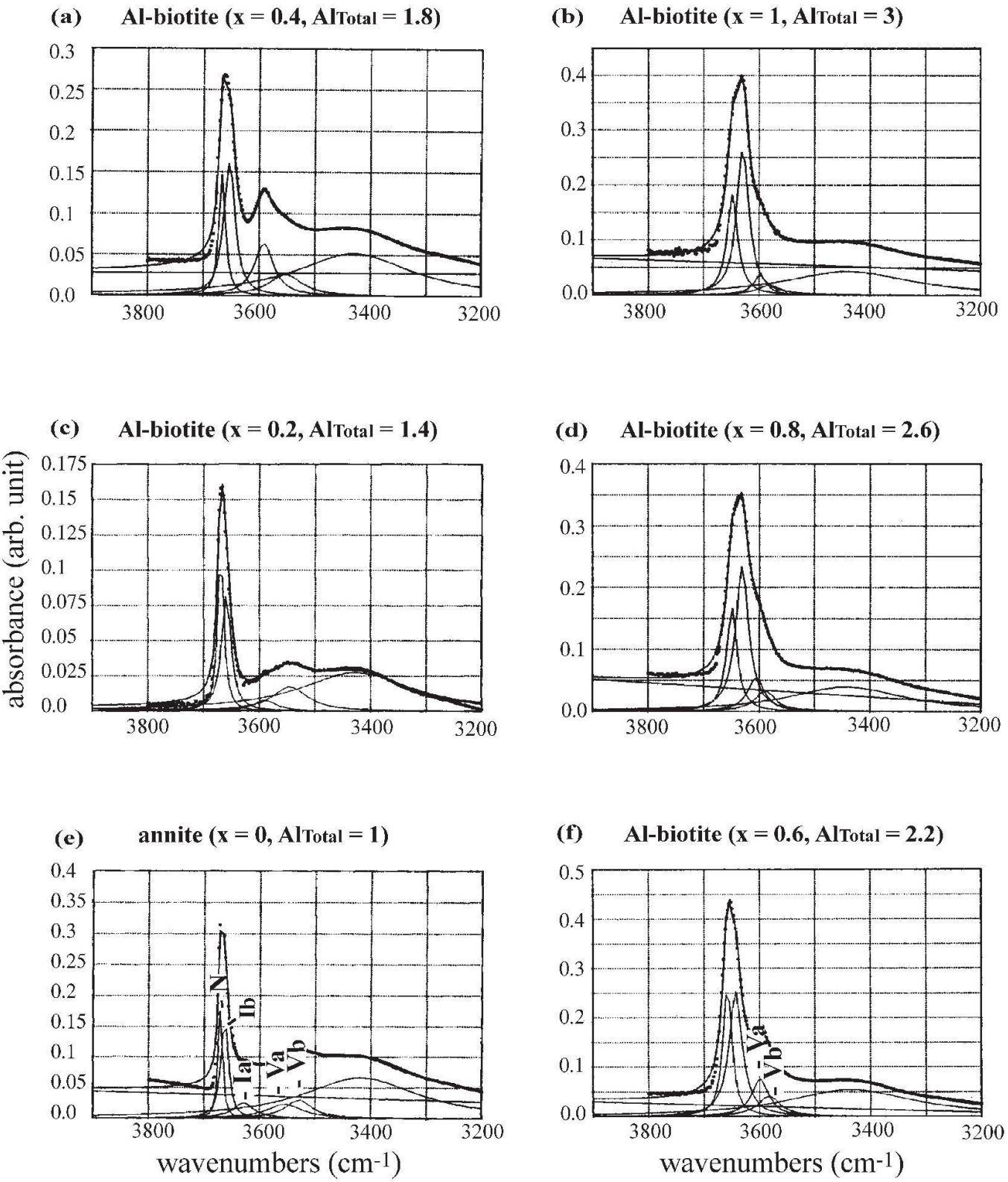

Fig. 3 Decomposed infrared spectra of micas along annite-siderophyllite join (600°C/MW/1 kbar). For meaning of bands see Fig. 2.

OH groups in the vicinity of two octahedrally coordinated Fe^{2+} and a vacancy (OH–$Fe^{2+}Fe^{2+}\square$).

Bands in the frequency range 3600–3520 cm^{-1}

Four V-bands have been identified in the low frequency range (3600–3520 cm^{-1}). In contrast to N- and I-type bands, the frequency of OH groups associated to vacancies increases with increasing x-value (increasing Al_{Total}, see Fig. 4). This results from the different orientation of OH groups and from the compositional variation of the mica (Robert and Kodama, 1988). Depending on the environment of the OH group, the band frequency decreases with increasing electronegativity of cations (χ) ($\chi Fe^{2+}Al^{3+}\square < \chi Fe^{2+}Fe^{3+}\square < \chi Fe^{3+}Al^{3+}\square$

<$\chi Fe^{3+}Fe^{3+}\square$). For annite, the highest frequency of V-bands is 3575 cm^{-1}. Vedder (1964) suggested that the frequency of OH groups such as OH–$M^{3+}M^{3+}\square$ (with $M^{3+} = Al^{3+}$ or Fe^{3+}) can be as high as 3650 cm^{-1}. In muscovite, the OH–$Al^{3+}Al^{3+}\square$ is observed at 3628 cm^{-1}. Bands assigned to OH–$Fe^{3+}Fe^{3+}\square$ occur at much lower frequencies than 3575 cm^{-1}. Thus, the V-band at 3575 cm^{-1} needs to be assigned to OH groups in an environment with $Fe^{2+}Al^{3+}\square$ (Di-5^{+}: dioctahedral environment with the bulk charge of cations 5^{+}, Va). This assignment is confirmed by the evolution of the band with changing Al_{Total} of the mica and changing fO_2: The intensity of the 3575 cm^{-1} band increases with increasing Al_{Total} of the mica (Fig. 2) and the decomposition of the spectrum of annite synthesized at low fO_2 (Fig. 3) did not reveal the presence of a band at 3575 cm^{-1}.

The decomposition of the annite spectrum shows that two additional V-bands are needed to model adequately the absorption spectrum in the range 3550–3525 cm^{-1}. A band Vb is observed at 3545 cm^{-1} in annite. Its frequency increases with increasing Al_{Total} up to approximately $Al_{Total} = 1.8$ (Fig. 4). For Fe-eastonite ($Al_{Total} = 2$), the frequency decreases slightly and increases again with increasing Al_{Total} (Fig. 4). This is interpreted to reflect two different environments of OH groups. The first environment (for low Al_{Total}) is assigned to a Vb-type band OH–$Fe^{3+}Fe^{2+}\square$ (Di-5^{+}) whereas the second environment (for high Al_{Total}) is assigned to a Vb' band OH–$Fe^{3+}Al^{3+}\square$. Finally, a band Vc with the lowest frequency at 3528 cm^{-1} is observed in the annite spectrum. This band cannot be distinguished for micas with $Al_{Total} > 1.4$ and at low fO_2 (Fig. 3). Therefore, this Vc-band is

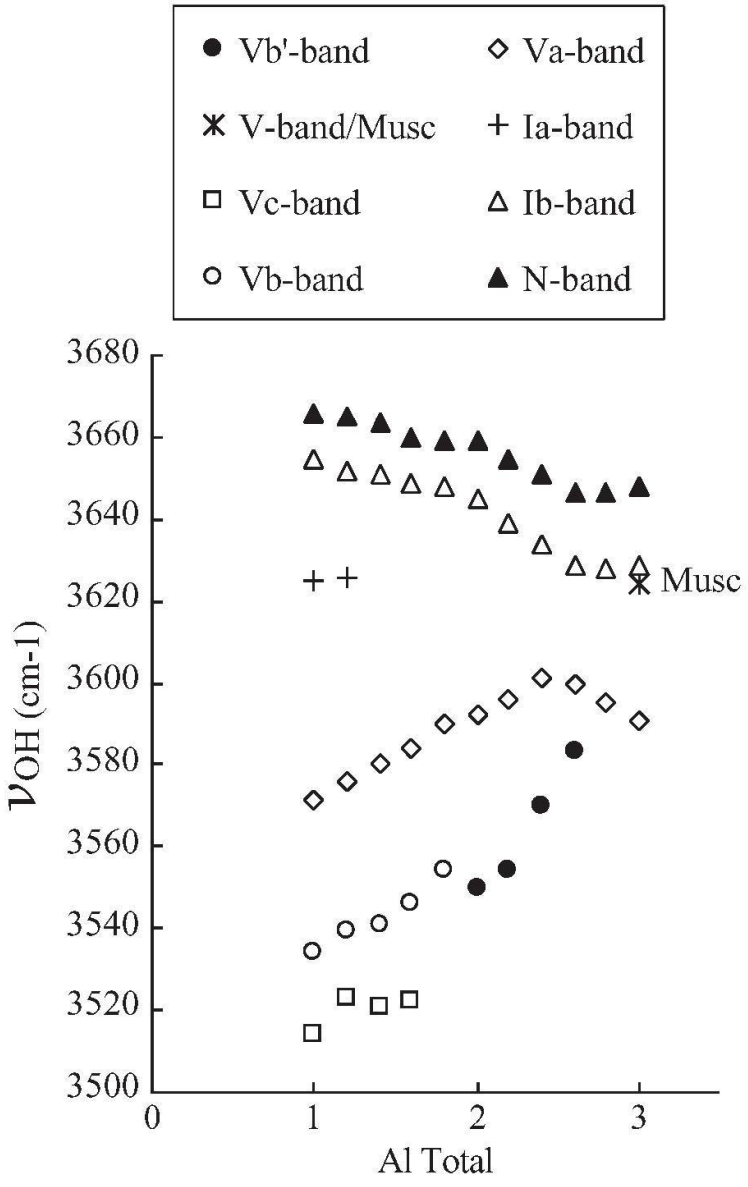

Fig. 4 Evolution of the OH-stretching wavenumbers (in cm^{-1}) of N, I and V-bands as a function of Al_{Total} from decomposed spectra of micas on the annite-siderophyllite join (600°C/NNO/1 kbar). For meaning of bands see Fig. 2. V-band/Musc refers to OH bonded to $Al^{3+}Al^{3+}\square$ of muscovite end-member.

assigned to $Fe^{3+}Fe^{3+}\square$ (Di-6$^+$). It can be noted that the assignment of the V-bands along the annite-siderophyllite join differs from previous ones. In particular, the Va-band at 3575 cm^{-1} has been assigned to OH associated to $Fe^{2+}Fe^{2+}Al^{3+}$ by Rancourt et al. (1994) and to OH–$Fe^{2+}Al^{3+}Al^{3+}$ by Levillain and Maurel (1980). For Al-rich biotites, Redhammer et al. (2000) assigned this band at 3580–3600 cm^{-1} to OH–$Fe^{2+}Al^{3+}Al^{3+}$ (Tri-8$^+$). This assignment needs to be reconsidered because it is not in agreement with the model of Robert and Kodama (1988, see Fig. 4), although Redhammer et al. (2000) assigned the bands on the basis of this model. In addition, an 8-fold charged environment is not common in micas. Up to now such an environment has only been recorded in Ti-rich phlogopite and Ti-rich biotite by Robert (1973) and Cesare et al. (2003), respectively.

Concluding remarks

The investigation of the evolution of infrared absorption bands along several compositions involving annite as end-member allows us to constrain empirically the role of compositional variations on the frequency and the intensity of these bands. This, coupled with the effects of the fO_2 on absorption bands, electronegativity of the cations adjacent to the hydroxyl groups, can be used to clarify the assignment of some characteristic absorption bands of trioctahedral micas and of annite in particular.

We show and argue that up to seven bands are observed in the infrared hydroxyl stretching region in micas along the annite-siderophyllite join: one N-type band, two I-type bands and four V-type bands ([$Fe^{2+}Al^{3+}\square$]; [$Fe^{3+}Fe^{2+}\square$]; [$Fe^{3+}Al^{3+}\square$]; [$Fe^{3+}Fe^{3+}\square$]; labeled Va, Vb, Vb'and Vc, respectively). An 8-fold charged environment OH–$Fe^{2+}Al^{3+}Al^{3+}$ (Tri-8$^+$) doesn't seem likely in these micas. At low fO_2, the spectrum of annite did not reveal the presence of a Vc-band.

The infrared spectra show that annite is a complex solid-solution which can also accommodate constituents such as ferri-muscovite and ferri-siderophyllite. The presence of Fe^{3+} and the substitution mechanism $3[^6]Fe^{2+} \Leftrightarrow 2[^6](Al^{3+}, Fe^{3+}) + [^6]\square$ may explain the limited extent of solid-solution observed along the annite-siderophyllite join.

Aknowledgements

I am very thankful and indebted to Dr. C. Levillain for these works on ferrous-aluminous biotites. The authors are grateful to Dr. E. Dachs and an anonymous referee for careful reviews of this manuscript.

References

Allred, A.L. and Rochow, E. (1958): A scale of electronegativity based on electrostatic force. *J. Inorg. Nucl. Chem.* **5**, 264–265.

Boukili, B. (1995): Cristallochimie des biotites ferro-alumineuses dans le système: Na_2O–K_2O–FeO–Fe_2O_3–Al_2O_3–SiO_2–H_2O–HF. Analyse par spectrométries vibrationnelles et Mössbauer. Thèse, Univ. Orléans, 320 pp.

Boukili, B., Robert, J-L. and Bény, J.-M. (1994): Characterization of trioctahedral micas solid solutions in the system: K_2O–FeO–Fe_2O_3–Al_2O_3–SiO_2–H_2O–HF by FTIR absorption and Mössbauer spectrometries. Symposium of International Mineralogy Association, Pisa, Italy, OSI-19.

Cesare, B., Cruciani, G. and Russo, U. (2003): Hydrogen deficiency in Ti-rich biotite from anatectic metapelites (El Joyazo, SE Spain): Crystal-chemical aspects and implications for high-temperature petrogenesis. *Am. Mineral.* **88**, 583–595.

Christanssen, C. (1884): Untersuchungen über die optischen Eigenschaften von fein verteilten Köpern. *Wiedemann Ann. Phys.* **23**, 298–306.

Cyang, G.L., Chou, I.M. and Sherman, D.M. (1996): Re-investigation of the annite = sanidine + magnetite + H_2 reaction using the fH_2 sensor technique. *Am. Mineral.* **81**, 475–484.

Dachs, E. (1994): Annite stability revised: 1. Hydrogen-sensor data for the reaction annite = sanidine + magnetite + H_2. *Contrib. Mineral. Petrol.* **117**, 229–240.

Donnay, G., Donnay, J.D.H. and Takeda, H. (1964): Trioctahedral one-layer micas. II. Prediction of the structure from composition and cell dimensions. *Acta Cryst.* **17**, 1341–1381.

Eugster, H.P. (1957): Stability of annite. Carnegie Institution of Washington Yearbook, 1956–57, 161–164.

Eugster, H.P. and Wones, D.R. (1962): Stability relations of the ferruginous biotites annite. *J. Petrol.* **3**, 82–126.

Farmer, V.C. (1974): The layer silicates. In: Farmer, V.C. (ed.): The infrared spectra of minerals. Mineral. Soc. London, 331–363.

Hamilton, D.L. and Henderson, C.B.M. (1968): The preparation of silicate compositions by gelling method. *Mineral. Mag.* **36**, 632–838.

Hazen, R.M. and Burnham, C.W. (1973): The crystal structure of one-layer phlogopite and annite. *Am. Mineral.* **58**, 889–900.

Levillain, C. (1982): Influence des substitutions cationiques et anioniques majeurs sur les spectres Mössbauer et Infrarouge des micas potassiques trioctaédriques. Applications cristallochimiques. Thèse d'Etat, Univ. Paris VI, 158 pp.

Levillain, C. and Maurel, P. (1980): Etude par spectrométrie infrarouge des fréquences d'élongation du groupement hydroxyl dans des micas synthétiques de la série annite-phlogopite et annite-siderophyllite. *C.R. Acad. Sci. Paris* **290**, 1289–1292.

Monier, G. and Robert, J.-L. (1986): Muscovite solid-solution in the system: K_2O–MgO–FeO–Al_2O_3–SiO_2–H_2O: An experimental study at 2 kbar PH_2O and comparison with natural Li-free white micas. *Mineral. Mag.* **50**, 257–266.

Nachit, H. (1986): Contribution à l'étude analytique et expérimentale des biotites des granitoïdes - applications typologiques. Thèse de 3ème cycle, Univ. Brest, 150 pp.

Rancourt, D.G., Christie, I.A.D., Royer, M., Kodama, H., Robert, J.-L, Lalonde, A.E. and Murad, E. (1994): Accurate $[^4]Fe^{3+}$ $[^6]Fe^{3+}$ and $[^6]Fe^{2+}$ site populations in synthetic annite by Mössbauer spectroscopy. *Am. Mineral.* **79**, 51–62.

Rebbert, C.R., Partin, E. and Hewitt, D.A. (1995): Synthetic biotite oxidation under hydrothermal conditions. *Am. Mineral.* **80**, 345–354.

Redhammer, G.J., Beran, A., Dachs, E. and Amthauer, G. (1993): A Mössbauer and X-Ray diffraction study of annites synthesized at different oxygen fugacities and crystal chemical implications. *Phys. Chem. Mineral.* **20**, 382–394.

Redhammer, G.J., Beran, A., Schneider, J., Amthauer, G. and Lottermoser, W. (2000): Spectroscopic and structural properties of synthetic micas on the annite-siderophyllite binary: Synthesis, crystal structure refinement, Mössbauer, and infrared spectroscopy. *Am. Mineral.* **85**, 449–465.

Robert, J.-L. (1973): Etude expérimentale de micas dans le système K_2O–MgO–TiO_2–Al_2O_3–SiO_2–H_2O. Thèse de 3éme cycle, Univ. Paris-Sud, 55 pp.

Robert, J.-L. (1981): Etudes cristallochimiques sur les micas et les amphiboles. Applications à la pétrographie et la géochimie. Thèse d'Etat, Univ. Paris XI Orsay, 206 pp.

Robert, J.-L. and Kodama, H. (1988): Generalization of the correlation between hydroxyl stretching wavenumbers and composition of micas in the system K_2O–MgO–Al_2O_3–SiO_2–H_2O: A single model for trioctahedral and dioctahedral micas. *Am. J. Sci.* **288-A**, 196–212.

Robert, J.-L Bény, J.-M., Bény, C. and Volfinger, M. (1989): Characterization of lepidolites by Raman and infrared spectrometries. Relations between OH-stretching, wavenumbers and compositions. *Can. Mineral.* **27**, 225–235.

Rousseaux, J.M., Gomez Laverde, Y., Nathan, Y. and Rouxet, P.G. (1972): Correlation between the hydroxyl stretching bands and the chemical compositions of the trioctahedral micas. Int. Clay Conf. Madrid, Preprint 1, 117–126.

Rouxet, P.G. (1970): Hydroxyl stretching bands in micas: A quantitative interpretation. *Clay Minerals* **8**, 375–388.

Rutherford, M.J. (1973): The phase relations of aluminous iron biotites in the system: $KAlSi_3O_8$–$KAlSiO_4$–Al_2O_3–Fe–O–H. *J. Petrol.* **14**, 159–180.

Sanderson, R.T. (1983): Electronegativity and bond energy. *J. Am. Chem. Soc.* **105**, 2259–2261.

Sanz, J. and Stone, W.E.E. (1983): NMR applied to minerals: VI. Local order in the octahedral sheet of micas: Fe-F avoidance. *Clay Minerals* **18**, 187–192.

Sanz, J., De La Calle, C. and Stone, W.E.E. (1984): NMR applied to minerals. V. The localization of vacancies in the octahedral sheet of aluminous biotites. *Phys. Chem. Mineral.* **11**, 235–240.

Vedder, W. (1964): Correlation between Infrared spectrum and chemical composition of micas. *Am. Mineral.* **49**, 736–768.

Velde, B. (1979): Cation-apical oxygen vibrations in mica tetrahedra. *Bull. Mineral.* **102**, 33–34.

Velde, B. (1983): Infrared OH-stretch bands in potassic micas, talcs and saponites; influence of electronic configuration and site of charge compensation. *Am. Mineral.* **68**, 1169–1173.

Wilkins, R.W.T. (1967): The hydroxyl-stretching region of biotite mica spectrum. *Mineral. Mag.* **36**, 325–333.

Wones, D.R. (1963): Physical properties of synthetic biotites on the join phlogopite-annite. *Am. Mineral.* **48**, 1300–1321.

Wones, D.R. and Eugster, H.P. (1965): Stability of biotite: experimental, theory and application. *Am. Mineral.* **50**, 1228–1272.

Received 19 January 2004
Accepted in revised form 13 April 2004
Editorial handling: T. Armbruster